Resonant Raman scattering by acoustic phonons in self-assembled quantum-dot multilayers: From a few layers to superlattices

M. Cazayous, J. Groenen, A. Zwick, A. Mlayah, and R. Carles
Laboratoire de Physique des Solides, UMR 5477, IRSAMC, Université P. Sabatier, 118 route de Narbonne, 31062 Toulouse Cedex 4, France

J. L. Bischoff and D. Dentel
Laboratoire de Physique et de Spectroscopie Electronique, UMR 7014, Faculté des Sciences et Techniques, 4 rue des Frères Lumière, 68093 Mulhouse Cedex, France

(Received 18 June 2002; revised manuscript received 25 September 2002; published 20 November 2002)

We report on resonant Raman scattering (RS) by acoustic phonons in self-assembled Ge/Si quantum-dot (QD) multilayers. In previous studies the observation of doublet features in the low-frequency Raman spectra was attributed to superlattice effects, i.e., Brillouin-zone folding, despite the often small number of QD layers. We propose a model which accounts for the low-frequency resonant RS, whatever the number of QD layers, i.e., from a few layers to superlattices. It is shown that the features in the low-frequency spectra (peak frequencies and intensities, doublet splittings and intensity ratios) can all be consistently understood within the resonant RS interference model. RS interferences occur when acoustic phonons interact with an ensemble of localized electronic states. Calculations and experiments were carried out in order to investigate how the RS depends on the number of QD layers and on the multilayer location with respect to the surface. Indeed, spectra are shown to depend on these finite-size effects: Reliable assignments cannot be made when the analysis is restricted to the peak frequencies. RS intensities have been calculated in order to identify the relevant scattering mechanism.

DOI: 10.1103/PhysRevB.66.195320 PACS number(s): 78.30.−j, 63.20.Kr, 81.07.Ta, 81.15.Hi

I. INTRODUCTION

Few studies on Raman scattering (RS) by acoustic phonons in self-assembled quantum-dot (QD) multilayers have been reported so far. Liu *et al.*[1] observed a series of peaks in the RS spectra of the Ge/Si QD superlattice (SL), which they attributed to scattering by acoustic phonons. Although several explanations were considered (multiphonon modes, superlattice related folded modes, and confined modes) in Yu's comment[2] on this work and in the response of Liu *et al.*[3] a definitive identification could not be provided. No spectra below 60 cm^{-1} were presented, however, and the signals were rather weak. The studies reported since do actually show that characteristic features are systematically observed in the low-frequency RS spectra. Tenne *et al.*[4] reported low-frequency Raman spectra of GaAs and AlAs QD's embedded in InAs. Although their samples contained only five QD layers, they observed peaks similar to those observed in planar superlattice spectra, the so-called doublets peaks which are related to folded acoustic phonons. The elastic continuum model commonly used for planar superlattices, i.e., Rytov's model,[5,6] was shown to predict the frequencies they observed. More recently, Milekhin *et al.*[7] did also observe the folded acoustic-phonon related peaks in resonant RS spectra of Ge/Si QD SL (which had actually ten QD layers). These peaks were however superimposed on a continuous emission. One may wonder why Rytov's model designed for infinite and planar multilayers accounts for the frequencies of the main features in spectra of finite multilayers QD's, i.e., containing three-dimensional nanostructures. It is not straightforward to identify which mechanism may induce this RS.

Here we propose a mechanism for the RS in QD multilayers. We believe that finding out a mechanism which accounts for the RS in QD multilayers whatever the number of layers, i.e., from a few layers to SL, is important indeed. We shall not limit this investigation to the frequency behavior. To identify a possible mechanism, electron-phonon interaction has to be considered explicitly (studies are often limited to the analysis of RS in terms of phonon frequencies). Huntzinger *et al.*[8] and Cazayous *et al.*[9] reported on low-frequency resonant RS measurements in single- and double-QD layers, respectively. Due to the three-dimensional electronic confinement, translational invariance is lost. Raman scattering by acoustic phonons then becomes allowed.[10–12] The interaction between acoustic phonons and confined electrons yields interferences.[9] The latter provide a means of probing spatial correlations in QD multilayers.[13]

The aim of this work is to show that these interferences may also account for the RS in structures containing many QD layers, i.e., QD SL's. We present RS spectra calculations. We shall discuss how the RS depends on the QD size, the spacing between QD layers, and the number of QD layers, and compare the simulations to experimental data.

II. EXPERIMENTS

Self-assembled Ge/Si QD multilayers were grown on Si(001) substrates by solid source molecular beam epitaxy at 600 °C. Growth was monitored in real time using a reflection high-energy electron-diffraction system, allowing to check the growth morphology. The multilayers were preceded by the deposit of a 50-nm Si buffer layer. The Stranski-Krastanov growth mode leads, after deposition of 6.5 Ge

monolayers, to the formation of hut islands having {105} facets and with a height-to-width ratio close to 1/10 before capping. Erosion of the island apex is limited during capping by choosing a high Si deposition rate.[14] As we intend to investigate here how the RS depends on the QD layer stacking (and not on the QD ordering), rather thin Si spacing layers were grown in order to obtain vertically ordered QD's. Samples *A*, *B*, and *C* contain 2, 5, and 20 QD layers, respectively. The Si spacing equals 18.5 nm for samples *A* and *B*, and 20 nm for sample *C*. Samples *A*, *B*, and *C* were capped with a 35-nm Si layer. Sample A' has the same characteristics as sample *A* but a 65-nm cap layer. The QD's have a typical height $h=6$ nm and width $w=80$ nm. The Ge content in the QD's is 75% as deduced from the RS by optical phonons.[15]

A T800 Coderg triple monochromator with a cooled GaAs photomultiplier was used for the low-frequency RS measurements. They were performed at room temperature and the samples were kept in vacuum in order to avoid air related Raman peaks. The excitation with the E_1 transition of the QD's was achieved with the 488-nm laser line of an argon laser. Notice that no specific confinement induced E_1 sublevels can be selected via resonance.[9,13]

III. MODEL

Raman spectra of QD multilayers were simulated using the model presented in Ref. 13. In this model we consider the deformation-potential interaction between an ensemble of spatially distributed confined electronic states and longitudinal acoustic modes. The resonant Raman intensity (Stokes scattering) is proportional to[13]

$$\left| \sum_{p,l_p} e^{i\Delta\vec{k}\cdot\vec{r}_{p,l_p}} \int \psi^*(\vec{r})[\vec{\nabla}\cdot\vec{u}(\omega,\vec{q})]\psi(\vec{r})d^3\vec{r} \right|^2. \qquad (1)$$

$\psi(\vec{r})$ is the electronic wave function which accounts for the confinement, p is the layer index, and l_p is the QD index within layer p. Δk is the difference between the incident and scattered photon wave vectors.

Due to the lack of translation invariance, the usual wave-vector conservation law does not hold here: all acoustic phonons may contribute to the Raman scattering. According to the three-dimensional confinement neither q_z nor $q_{||}$ are conserved.

The coherent sum of the scattering amplitudes yields interferences; oscillations are observed in the low-frequency resonant RS spectra.[9,13] Two terms can be identified in the RS intensity: a form factor and a structure factor.

(i) The form factor is related to the Fourier transform of the electronic density inside a QD and determines the spectral envelope of the interference oscillations. In the frequency range investigated here, the acoustic-phonon dispersion is linear. The spectral extent of the RS is thus simply related to the QD dimensions. Here, according to the QD shapes, the envelope is mainly determined by the QD height.

(ii) The structure factor includes the relative QD positions and determines the interference oscillation period and contrast. Ordered QD's yield maximum interference contrast.

QD's are modeled by quantum disks, including thus in-plane and vertical confinement. The QD distribution considered in the simulations are vertically correlated but random in plane. Acoustic phonons with both wave-vector components in-plane and along the growth direction are considered. According to the QD height/width ratio, the acoustic phonons that contribute significantly to the signal have small in-plane wave-vector components. They were calculated considering displacement and stress continuities at the interfaces, i.e., acoustic wave reflections at the interfaces and also at the sample surface. In each layer, the appropriate sound velocities (v_{QD} and v_{Si}) and densities (ρ_{QD} and ρ_{Si}) are considered. Further details on the simulations can be found in Ref. 13.

Simulations are performed using Eq. (1). We shall however provide here a simplified but useful expression for the structural factor. Let us assume (unlike in the simulations) that one can describe an acoustic mode using a single—average or effective—sound velocity v. We shall focuss on the part of the structural factor related to the growth axis z. Unlike the structural factor given in Ref. 13, we shall present here the contributions of the two counterpropagating components of each acoustic mode (labeled $+q_z$ and $-q_z$ for the component propagating away and towards the sample surface, respectively) and the difference between incident and scattered photon wave vectors $\Delta k_z = k_{i,z} - k_{s,z}$. After performing the coherent sum over the N QD layers, one finds that the RS interference structural factor is proportional to

$$H^2(\Delta k_z + q_z) + H^2(\Delta k_z - q_z) - 2H(\Delta k_z + q_z) \times H(\Delta k_z - q_z)\cos[q_z\{(2z_1 + (N-1)t\}], \qquad (2)$$

where t is the spacing between QD layers and H is the usual interference function,[16]

$$H(Q) = \frac{\sin\left(\frac{Nt}{2}Q\right)}{\sin\left(\frac{t}{2}Q\right)}. \qquad (3)$$

The first term in Eq. (2) is related to the $+q_z$ component and the second one to $-q_z$. The contributions of $+q_z$ and $-q_z$ components are different. Indeed, intensity maxima are obtained for

$$(\Delta k_z \pm q_z)\frac{t}{2} = \pi n, \qquad (4)$$

where n is a relative integer. The third term in Eq. (2) includes contributions of both components and depends on the position z_1 of the first QD layer with respect to the sample surface. Equation (2) allows to point out easily the QD layer stacking and the surface effects to be discussed below.

IV. SIMULATIONS AND EXPERIMENTAL RESULTS

A. Stacking effects

Figure 1 shows low-frequency Raman spectra calculated for an interlayer spacing $t=15$ nm and the number of QD

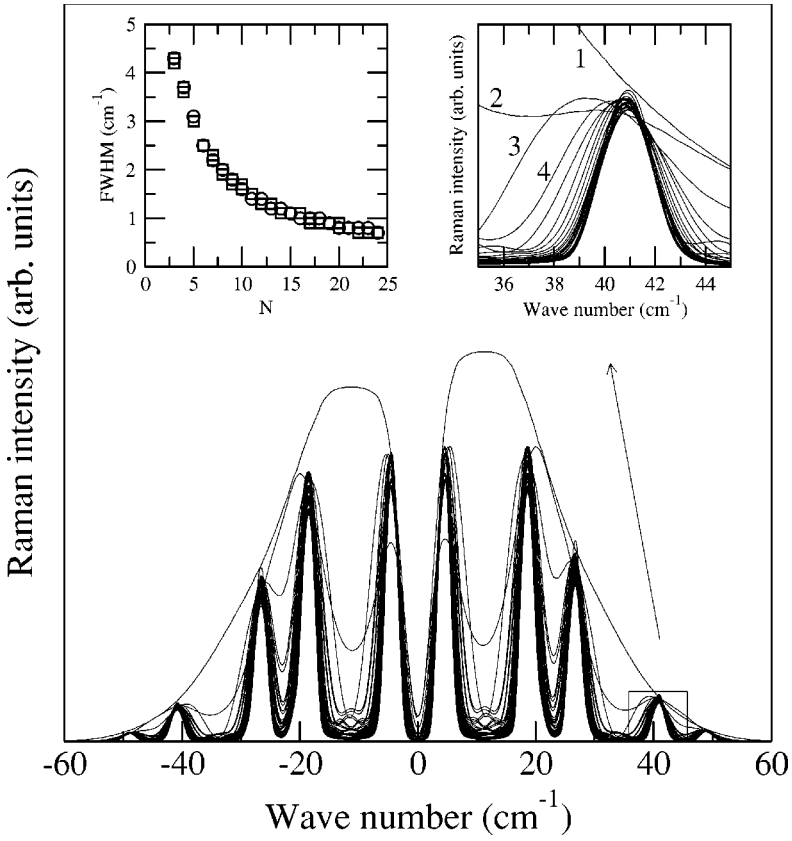

FIG. 1. Simulated resonant Raman spectra for N ranging from 1 to 25 for a given spacing $t = 15$ nm. Arbitrary scaling factors were used in order to enable observation of the changes in the spectra. The left inset shows the full width at half maximum (FWHM) of the two first peaks as a function of N (square and circle, respectively). The right inset is an enlargement, showing the changes for small N values ($N=1-4$).

layers N ranging from 1 to 25. The QD height and diameter are equal to 6.5 nm and 80 nm, respectively. A large final cap layer ($z_1 = 1$ μm) was considered to avoid surface effects (to be discussed in Sec. IV C). In order to further compare with the experimental results the theoretical spectra have been convoluted with the spectral reponse of our experimental setup (2 cm^{-1} resolution).

The form factor is obtained for $N=1$. This spectrum is related to the Fourier transform of the electronic density. The smaller the QD's the more the envelope spreads out.[17] This spectrum displays a typical signature of the three-dimensional electronic confinement: because phonons with both q_z and $q_{||}$ wave-vector components are involved, the spectrum vanishes for $\omega \rightarrow 0$.[11,12]

For $N>1$, the spectra display periodic oscillations. The envelope of these oscillations is the previous form factor ($N=1$). Intensity maxima (minima) correspond to constructive (destructive) interferences comparable to the well-known bright and dark fringes in optics. The spectra display doublet features; notice that they start forming for $N=2$. These doublets are due to the two first terms in Eq. (2). The phase conditions yielding maxima differ for the $+q_z$ and $-q_z$ components of a given vibrational mode, i.e., given wave number. Let us now consider the whole spectrum, i.e., different wave numbers. Maxima appear at different wave numbers for the first and second terms in Eq. (2): doublets appear. According to Eq. (3), the interference period varies as $1/t$. The peak frequencies and doublets splitting depend on Δk_z, whereas the period does not. Δk_z is determined by the scattering geometry. The relative peak intensities within a given doublet or between doublets are determined by the interference envelope (i.e., the electronic confinement) and the acoustic impedance mismatch (here $\eta = \rho_{\mathrm{Si}} v_{\mathrm{Si}} / \rho_{\mathrm{Ge}} v_{\mathrm{Ge}} = 0.78$). According to the interference function H, when N increases peaks get sharper (see inset Fig. 1) and weak secondary intensity maxima appear.

In infinite and periodic multilayers (i.e., SL) the Brillouin zone is folded into a minizone (delimited by $q=0$ and $q_m = \pi/d$) and phonon energy gaps are opened at the minizone boundaries. Rytov's model is usually used to calculate the acoustic-phonon dispersion within the SL Brillouin minizone $\omega(q_{SL})$. The SL dispersion relation derived in Rytov's model can be written in the following simplified form (assuming no acoustic mismatch):[18]

$$\omega = v\left(\pm q_{SL} + 2\pi \frac{m}{t} \right), \tag{5}$$

where v is the mean sound velocity and m the folding index.[19]

Even in multilayers containing only very few QD layers, oscillations of the low-frequency RS are well defined. We emphasize that neither the peaks nor the doublets are due to Brillouin-zone folding, phonon energy gaps, or accumulations in the phonon density of states.[20,21] Our calculations deal with finite-size structures (similar to those investigated experimentally). No phonon energy gaps are opened. Phonon energy gap opening requires multiple constructive wave reflections, i.e., many layers.[20] Assuming an infinite multilayer, one would obtain small phonon energy gaps ($\simeq 1.2$ cm^{-1}) at the minizone boundaries.

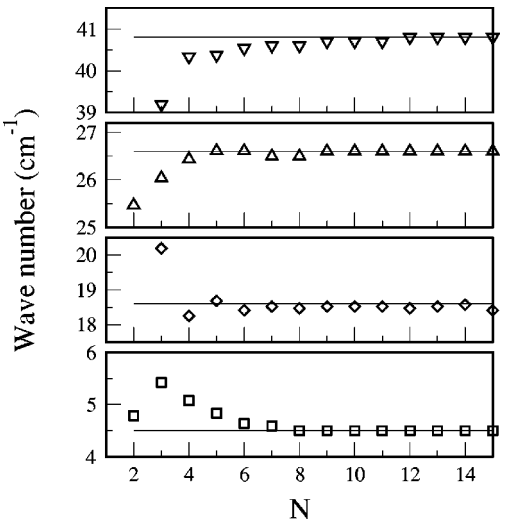

FIG. 2. Frequencies of the interference maxima (bright fringes) in Fig. 1 as a function of the stack number *N*. Straight lines are the frequencies derived from Rytov's model assuming a superlattice.

Moreover, one can notice small frequency changes of the intensity maxima when *N* increases (Fig. 1). The frequencies tend however rapidly towards those predicted by Rytov's model (Fig. 2). These frequencies were derived from the SL minizone dispersion, considering the phonon wave vector $q_{SL}=\Delta k_z$ given by the momentum conservation for the backscattering geometry in a SL.[22] Deriving the intensity maximum positions from Eq. (4) (with $\omega=vq_z$) or from Eq. (5) (with $q_{SL}=\Delta k_z$) yields the same wave numbers. As soon as defining a mean velocity makes sense (i.e., for large *N* values), the momentum conservation for SL and the constructive interference condition are equivalent (as far as peak positions are concerned). For small *N* values, the simulations predict small frequency changes. Equation (2) does not hold; one has to consider the sound velocities v_{QD} and v_{Si} in the QD and Si layers. Our simulations show that the frequencies predicted by Rytov's model are already recovered for small *N* values ($N\geqslant 5$). If one omits the peak narrowing (inset in Fig. 1), no major changes in the spectral shape occur when *N* further increases.

Figure 3 shows how spectra depend on the spacing between QD layers for a given number of layers $N=20$ ($h=3$ nm and $w=30$ nm). Increasing *t* reduces the interference oscillation period, as expected. According to the large number of QD layers, the frequencies of the intensity maxima can be derived from Rytov's model.[23] Although the Brillouin-zone folding scheme is not valid, it allows to easily understand how the peaks shift and merge together. Changing *t* is equivalent to exploring minizone dispersion branches. The doublet splitting depends much on the QD layer spacing too. It is worth noting that when the interference oscillation period is comparable to the doublet splitting (upper part of Fig. 3), oscillations have only a small contrast, even when the QD's are vertically correlated.[13]

B. Comparaison with experiment

Figure 4 shows calculated and measured resonant Raman

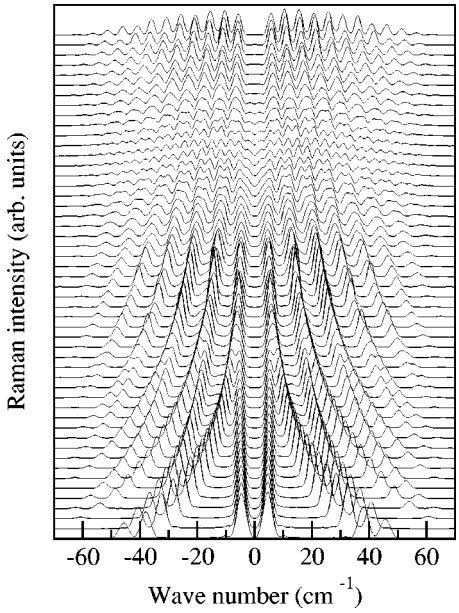

FIG. 3. Simulated Raman spectra for interlayer spacing ranging from 5 to 105 nm with a step of 2 nm ($N=20$).

spectra of the structures consisting of 2, 5, and 20 QD layers (samples *A*, *B*, and *C*). As expected, doublets features are observed and peaks get sharper when *N* increases. The calculations account rather well for the peak frequencies, doublets splitting, and relative intensities within a doublet and between doublets. The spectral envelope of the low-frequency oscillations depends on the QD height and width.[13] Such size effects were already reported and discussed in Ref. 17.

Figure 5 shows how the interference oscillation period and doublet splitting depend on the QD layer spacing. Experimental data from sample *B* and Ref. 13 ($N=5$, *h*

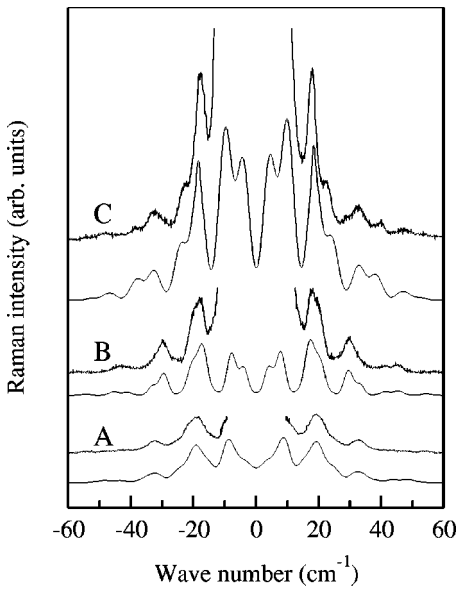

FIG. 4. Experimental and simulated resonant RS spectra for samples *A*, *B*, and *C* ($N=2$, 5, and 20, respectively).

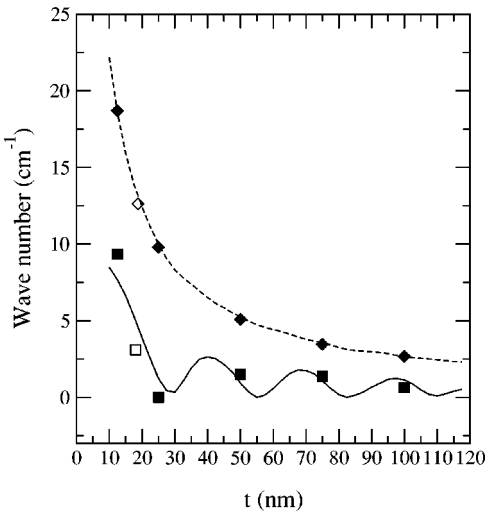

FIG. 5. Oscillation period (dashed line) and doublet splitting (straight line) as a function of spacing t for the number of layers $N=5$. Open and filled symbols are experimental data from sample B and Ref. 13, respectively.

$=6$ nm, $w=85$ nm) are included in Fig. 5. Again good agreement is obtained. Notice the beats in the doublet splitting.

C. Surface effects

Surface effects are related to the last term of Eq. (2). This term appears because in each layer two counterpropagating wave components are considered. These components are linked together due to reflections at Ge/Si interfaces and the sample surface. Notice that the reflection coefficient of a sound wave at the Ge/Si interface is very small ($\approx 1\%$). One expects an additional modulation; its period varies as $1/[z_1 + (N-1)/2t]$ [Eq. (2)], i.e., inversely with the distance between the surface and the middle of the QD layer stack.

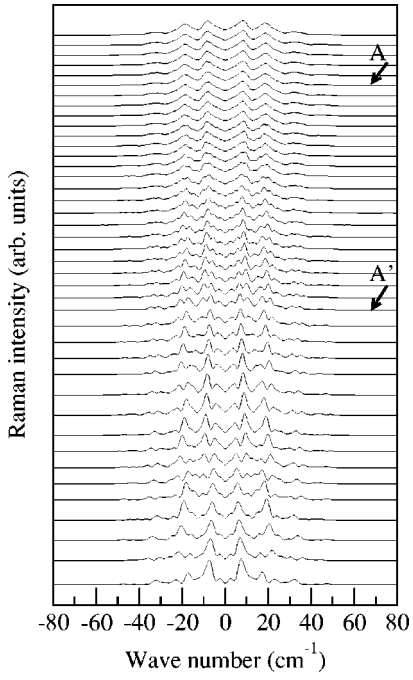

FIG. 6. Simulated Raman spectra for $N=2$ and $t=18.5$ nm with z_1 being the distance between the first QD layer and the sample surface ranging from 11 up to 72.5 nm (from bottom to top). The arrows indicate the spectra corresponding to samples A and A'.

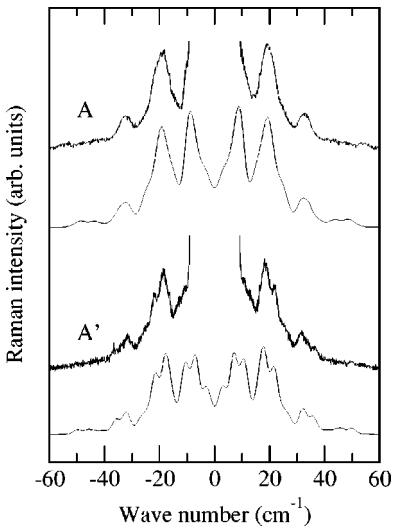

FIG. 7. Experimental and simulated Raman spectra for samples A and A' ($N=2$). The caplayer thickness z_1 is 65 and 35 nm, respectively.

In order to point out the surface effects we performed simulations with z_1 varying from 11 up to 72.5 nm. In order to maximize the role of the surface, we choose a double-QD-layer structure. These simulations are reported in Fig. 6. With respect to the simulations discussed so far, an additional periodic intensity modulation is observed, indeed. This modulation is not resolved for thick cap layers (upper part of Fig. 6) but modifies significantly the spectra when the cap layers are thin (lower part of Fig. 6). Although the spacing is kept constant, the apparent maxima shift when the cap layer thickness changes. One should not confuse these small oscillations with the doublets discussed above. Arrows in Fig. 6 indicate the spectra corresponding to samples A and A'. Figure 7 shows that the simulations compare well with the experimental data. Obviously, the observation of this modulation is definitely a finite-size effect and demonstrates that the interference model in which surface effects are included provides a relevant description.

According to Eq. (2), oscillations are expected even in the low-frequency spectra of single-QD-layer structures: these oscillations are related to the acoustic wave reflection at the sample surface and their period varies as $1/z_1$. These features were indeed observed experimentally.[8] These oscillations can be viewed as interferences between the QD layer and its acoustic image with respect to the sample surface.

For structures having thin cap layers but containing many QD layers, these oscillations can hardly be resolved (see Fig. 4). Indeed, when N increases, the modulation period and the overlap between $H(\Delta k_z + q_z)$ and $H(\Delta k_z - q_z)$ decrease.

V. DISCUSSION

The good agreement between the simulations and the experiments suggests that RS interferences are relevant for

resonant RS in QD multilayers. Intensities (including ratios and fine structures) are well accounted for. Moreover, this comparison shows that the same mechanism is able to account for the RS in structures with small and large stack numbers. It was shown that Rytov's model and the constructive interference condition yield the same peak frequencies already for rather small N values. Significant differences have to be pointed out however. First, in planar SL, the superperiodicity opens gaps in the acoustic-phonon dispersion relation at Bragg wave vectors (due to the constructive phonon wave reflection at the interfaces) and the Brillouin zone can be folded. Because of superperiodicity, momentum is conserved in the scattering process and sharp peaks (doublets) are observed. In the interference scheme no periodicity is required. Momentum is not conserved and peaks appear because of constructive interferences. Second, doublet peaks and the gap opening originate in Rytov's model only due to the difference between the acoustical properties of the two materials. In our model, even with identical acoustic properties, one would obtain low-frequency oscillations which are only due to interferences.

Milekhin *et al.*[7] reported the simultaneous observation of oscillations and a broad continuous emission. They suggested that the oscillations are superimposed on the continuous emission, attributing the appearance of those signals to different mechanisms: oscillations were assigned to folded acoustic phonons and the continuous emission was explained in terms of the breakdown of the crystal momentum conservation. We suggest that the oscillations are not superimposed on the continuous emission. Indeed, within the interference scheme, the oscillations and continuous emission are part of the same RS signal. Their simultaneous observation may be due to interferences with a limited or reduced interference contrast.

The application of the model presented here to the structures investigated in Ref. 4 would be questionable. Indeed, Ref. 4 deals with GaAs and AlAs dots embedded in InAs. Since the matrix has a smaller band gap, one does not expect confined electronic states in the self-assembled islands. The model presented here involves localized electronic states and deals with resonant RS. In experiments, one has to carefully identify which electronic states are involved. One should note that the low-frequency measurements presented in Ref. 4 were recorded in the vicinity of the E_1 transition of InAs, i.e., the barriers.[24]

Finally, we would like to compare the model presented here and the photoelastic model widely used to calculate low-frequency off-resonance RS of planar SL.[21,25] RS is described in terms of polarizability modulation due to the photoelastic effect. In the photoelastic model, RS in multilayers is treated as a coherent sum of scattering within bulklike layers. The scattering efficiency within each layer is included by means of photoelastic constants[26] [instead of the electron-phonon interaction in Eq. (1)]. There is a similarity between the two models: contributions of the different layers are summed coherently. The form factor (related to the electronic confinement) and the photoelastic constants play equivalent roles. They determine, in particular, the relative intensities between doublets.[27] Notice that considering very different photoelastic constants (for instance, $P_{\mathrm{Ge}}=10$ and $P_{\mathrm{Si}}=1$, in Ref. 21) is equivalent to considering localized electronic states (with a step profile) in our model. Obviously both models may thus provide similar results whereas the description of the scattering process is different. Most of the spectra are, however, recorded under resonance conditions. In particular, Ge/Si E_1 resonances are known to be very broad.[31]

VI. CONCLUSION

We have shown that RS interferences account for the resonant low-frequency Raman spectra of QD multilayers. We emphasize that, within the interference scheme, there is no need to assume the folding of the acoustic-phonon dispersion curve, i.e., superperiodicity. This assumption would be highly questionable indeed for small stacks, such as those often investigated experimentally. Our simulations explain the observation of doublet peaks reported in previous studies. This low-frequency RS originates from the three-dimensional electronic confinement in the QD's. The latter is therefore explicitly considered in the RS simulations. Electronic confinement determines the interference envelope and thus the relative peak intensities. The QD layer stacking determines the interference oscillation period, the QD distribution within the layers, and the interference contrast. Whatever the number of QD layers—small stacks or superlattices—the simulations and experiment compare well. Frequencies, intensities, and width are well accounted for.

[1] J.L. Liu, G. Jin, Y.S. Tang, Y.H. Luo, K.L. Wang, and D.P. Yu, Appl. Phys. Lett. **76**, 586 (2000).
[2] P.Y. Yu, Appl. Phys. Lett. **78**, 1160 (2001).
[3] J.L. Liu, G. Jin, Y.S. Tang, Y.H. Luo, K.L. Wang, and D.P. Yu, Appl. Phys. Lett. **78**, 1162 (2001).
[4] D.A. Tenne, V.A. Haisler, A.I. Toropov, A.K. Bakarov, A.K. Gutakovsky, D.R.T. Zahn, and A.P. Shebanin, Phys. Rev. B **61**, 13 785 (2000).
[5] S.M. Rytov, Akoust. Zh. **2**, 71 (1956) [Sov. Phys. Acoust. **2**, 68 (1956)].
[6] C. Colvard, R. Merlin, M.V. Klein, and A.C. Gossard, Phys. Rev. Lett. **45**, 298 (1980).
[7] A.G. Milekhin, A.I. Nikiforov, O.G. Pchelyakov, S. Schulze, and D.R.T. Zahn, JETP Lett. **73**, 461 (2001); Nanotechnology **13**, 55 (2002).
[8] J.R. Huntzinger, J. Groenen, M. Cazayous, A. Mlayah, N. Bertru, C. Paranthoen, O. Dehaese, H. Carrère, E. Bedel, and G. Armelles, Phys. Rev. B **61**, R10 547 (2000).
[9] M. Cazayous, J.R. Huntzinger, J. Groenen, A. Mlayah, S. Christiansen, H.P. Strunk, O.G. Schmidt, and K. Eberl, Phys. Rev. B

62, 7243 (2000).
[10] V.F. Sapega, V.I. Belitsky, T. Ruf, H.D. Fuchs, M. Cardona, and K. Ploog, Phys. Rev. B **46**, 16 005 (1992).
[11] T. Ruf, J. Spitzer, V.F. Sapega, V.I. Belitsky, M. Cardona, and K. Ploog, Phys. Rev. B **50**, 1792 (1994).
[12] V.I. Belitsky, T. Ruf, J. Spitzer, and M. Cardona, Phys. Rev. B **49**, 8263 (1994).
[13] M. Cazayous, J. Groenen, J.R. Huntzinger, A. Mlayah, and O.G. Schmidt, Phys. Rev. B **64**, 033306 (2001).
[14] L. Kubler, D. Dentel, J.L. Bischoff, G. Ghica, C. Ulhacq-Bouillet, and J. Werckmann, Appl. Phys. Lett. **73**, 1053 (1998).
[15] J. Groenen, R. Carles, S. Christiansen, M. Albrecht, W. Dorsch, H.P. Strunk, H. Wawra, and G. Wagner, Appl. Phys. Lett. **71**, 3856 (1997).
[16] M. Born and E. Wolf, *Principles of Optics: Electromagnetic Theory of Propagation, Interference and Diffraction of Light* (Pergamon Press, London, 1959).
[17] M. Cazayous, J. Groenen, J.R. Huntzinger, A. Mlayah, U. Denker, and O.G. Schmidt, Mater. Sci. Eng., B **88**, 63 (2002).
[18] D.J. Lockwood, M.W.C. Dharma-Wardana, J.-M. Baribeau, and D.C. Houghton, Phys. Rev. B **35**, 2243 (1987).
[19] J. Sapriel, J. He, B. Djafari-Rouhani, R. Azoulay, and F. Mollot, Phys. Rev. B **37**, 4099 (1988).
[20] O. Pilla, V. Lemos, and M. Montagna, Phys. Rev. B **50**, 11 845 (1994).
[21] M.W.C. Dharma-Wardana, P.X. Zhang, and D.J. Lockwood, Phys. Rev. B **48**, 11 960 (1993).
[22] Notice that this wave vector ($q \approx 0.77 q_m$) lies well inside the minizone, away from the phonon energy gaps and accumulations in the phonon density of states.
[23] V.F. Sapega, V.I. Belitsky, A.J. Shields, T. Ruf, M. Cardona, and K. Ploog, Solid State Commun. **84**, 1039 (1992).
[24] R. Carles, N. Saint-Cricq, J.B. Renucci, A. Zwick, and M.A. Renucci, Phys. Rev. B **22**, 6120 (1980).
[25] C. Colvard, T.A. Gant, M.V. Klein, R. Merlin, R. Fischer, H. Morkoc, and A.C. Gossard, Phys. Rev. B **31**, 2080 (1985).
[26] M.W.C. Dharma-Wardana, D.J. Lockwood, J.-M. Baribeau, and D.C. Houghton, Phys. Rev. B **34**, 3034 (1986).
[27] Photoelastic constants were often fitted to account for the doublets intensities; various values have been reported.[28–30]
[28] J. He, J. Sapriel, J. Chavignon, R. Azoulay, L. Dugrand, F. Mollot, B. Djafari-Rouhani, and R. Vacher, J. Phys. C **48**, 573 (1987).
[29] B. Jusserand, D. Paquet, F. Mollot, F. Alexandre, and G. Le Roux, Phys. Rev. B **35**, 2808 (1987).
[30] M. Cardona and G. Güntherodt, *Light Scattering in Solids V: Superlattices and Other Microstructures* (Springer, Berlin, 1989).
[31] M. Renucci, J.B. Renucci, and M. Cardona, Solid State Commun. **9**, 1235 (1971).